Paper 6.4

Fine Scale Mapping of the Manhattan Heat Island for Health Impacts

Brian Vant-Hull, Maryam Karimi, Mark Arend, Rouzbeh Nazari, Reza Khanbilvardi
NOAA-CREST, The City College of New York

Abstract: The definitive urban environment, Manhattan hosts a variety of micro-environments defined by parks, varying building heights, and proximity to water bodies. Fine scale temperature and humidity maps are necessary to understand how this variation on the neighborhood scale affects variations in microclimate. Backpack mounted data loggers have been deployed in a series of simultaneous parallel walks to measure temperature and humidity at rougly 10 meter intervals, categorized by segments of shade and direct insolation. Roughly 30 such campaigns should be completed by the end of the summer of 2013. The measurements are detrended in time against fixed meteorological stations, then normalized by the daily Manhattan-wide averages and standard deviations. 10 fixed stations have also been located throughout Manhattan measuring temperature and humidity at 3 minute intervals to capture convective and turbulent variations. The data show local temperature anomalies on the scale of several hundred meters that change location from day to day and are ascribed to the convective structure of the atmosphere. Upon averaging multiple days together the convective structure disappears and the remaining signal appears to be most strongly correlated to elevation and building height. The resulting temperature and humidity maps will be used for multiple variable regression against local variables of vegetation, building characteristics, albedo, water proximity and elevation to arrive at a formula for predicting micro variations in the urban heat island. Intended applications are predicting and mitigating heat related mortality.

Introduction

Most studies of the urban heat island (UHI) have focussed on the elevation of urban over rural temperatures, a difference that peaks at night due primarily to higher heat storage and nocturnal release; and to radiative trapping in urban canyons [Oke, 1982; Grimmond and Oke, 1999]. Yet city inhabitants would be more concerned with temperature differences within the 'urban archepelago' caused by variations in building structure, vegetation, and elevation; differences that can be as high as several degrees Centigrade [Yamashita, 1996; Weng et al, 2003, 2008; Stewart et al, 2003; Rosensweig et al, 2006; Pena, 2009; Montavez et al, 2000; Grimmond, 2007; Gaffin et al, 2008; Eliasson, 1996a,b; Comrie, 2000; Bottyan and Unger, 2003]. This pattern could affect heat related mortality during heat waves, which rises quasi-exponentially with temperature so that the health impacts becomes sensitive to such small variations [Kinney et al, 2008a,b].

Corresponding author: brianvh@ce.ccny.cuny.edu, NOAA-CREST, Steinman Hall, City College of New York, New York, NY, 10031.

Measurements of the UHI can be done at high spatial resolution using mobile sensors, over long time periods using fixed instruments, or by remote sensing. Both mobile and remote sensing techniques tend to be episodic so may not capture the range of meteorological variatiability, while fixed instrumentation typically has coarse spatial resolution. Satellite measurements capture a range of street level and rooftop temperatures, and measure surface rather than air temperature [Pena, 2009; Rosenzweig et al, 2006; Weng and Schubring, 2003; Weng et al, 2008; Weng, 2009]. For this work a combination of fixed and mobile instrumentation has been employed to capture the street level variation of Manhattan's heat island.

Instrumentation and Data Collection

Figure 1a is a LandSat Google Earth image of Manhattan, with pedestrian routes marked in yellow and fixed instrument locations marked with orange boxes. This RGB image portrays a sense of the variation in vegetation, albedo, building size and density on the island. The axis of Manhattan is tilted, with *streets* running roughly East-West (the street names of the various routes are labelled in white) and *avenues* running roughly North-South,

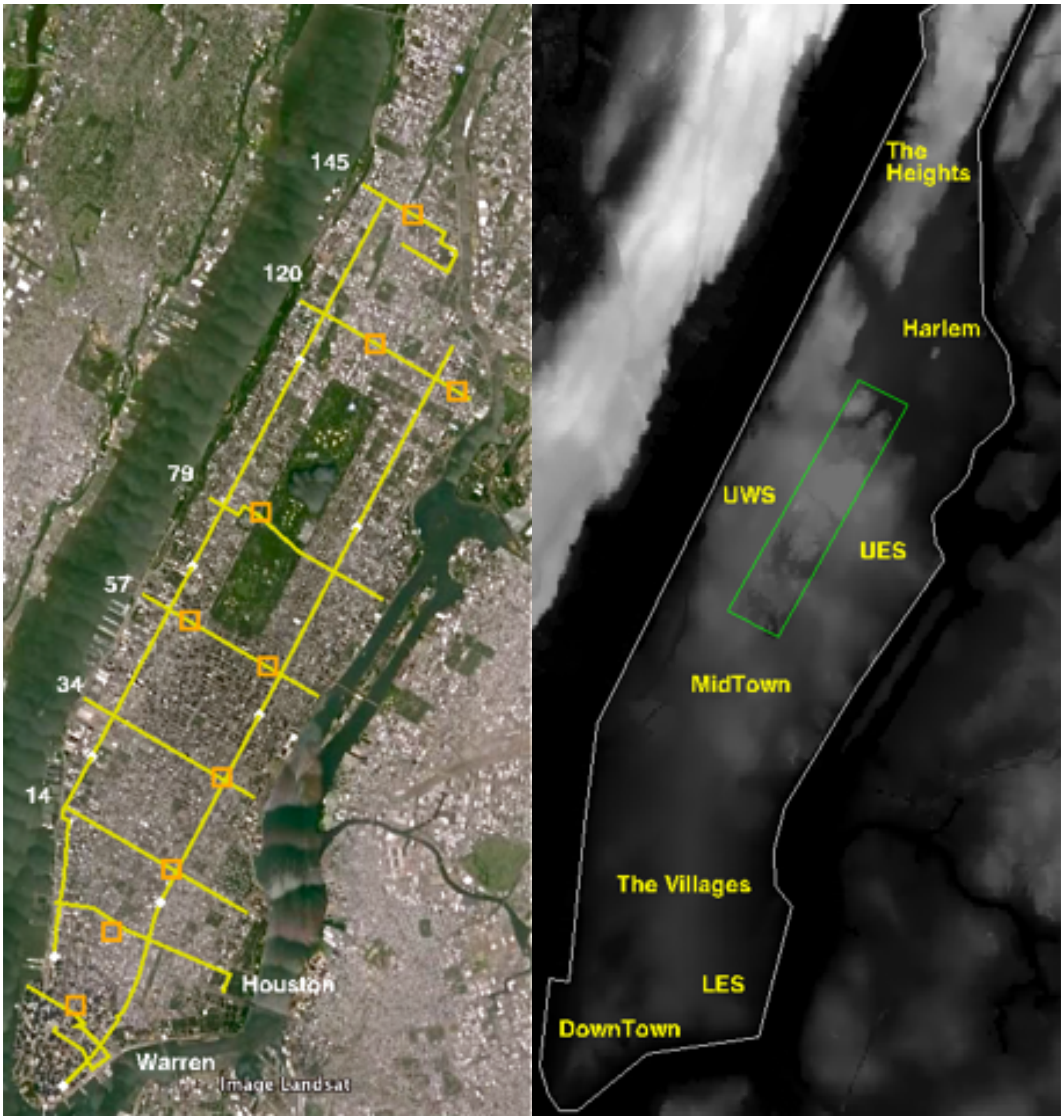

Figure 1: Mobile instrument pedestrian routes and fixed instrument locations (left). Elevations and neighborhoods (right).

bounded by the Hudson river and the East river. Due to the inclination, at the time of the walks (between and 2 and 3 PM) the sun would be shining directly down the avenues, while pedestrians on the south side of the streets would be in shade.

Elevation also affects air temperature, and Figure 1b portrays elevation in grayscale, with the main neighborhoods and Central Park marked. Elevations generally range from 1 to 2 meters above sea level near the rivers, up to 30 meters in parts of Central Park and 35 meters in the heights. The Villages, Lower East Side (LES), Harlem and the heights generally have buildings of 7 stories or less, while Downtown, Midtown, and the southern portions of the upper East and West sides tend towards highrises and skyscrapers.

Mobile Instrument Campaigns

Eight Vernier Corporation portable data loggers with temperature and relative humidity sensors were deployed simultaneously along parallel routes along prescribed street or avenue routes of Manhattan as shown in Fig. 1 a, starting at 2 pm and continuing along routes of equal distance (approximately 3 km or 40 minutes). The instrumentation was chosen for the fast response time of the Vernier surface temperature sensor, allowing high resolution temperature measurements. Dewpoint was calculated from temperature and relative humidity via the Magnus formula [Aldukov and Eskridge, 1996]. The larger thermal mass of RH sensor introduced dewpoint biases if the temperature changed quickly, largely mitigated by the averaging procedure described below.

The instruments were mounted on white cardboard with the measurement tips shielded from radiation by a styrofoam cup. These instruments packs were deployed on backpacks at a uniform height of 1.5 meters, with clothing or books inside to insulate the instruments from body heat. Measurements were taken every 10 seconds, corresponding to every 10 to 20 meters at walking speeds of between 1 and 2 m/s. The fixed distances of the routes were divided into 20 segments by equal time, within which data was averaged. For straight, uniform routes equal times would mean equal distances, but routes that had large changes in elevation or street crossings were navigated with cellphone geo-location (GPS is not feasible given Manhattan's tall buildings) to capture varying walking rates in different segments of the route. These segments were roughly 2 minutes in length, or 150 meters.

8 street walks and 2 avenue walks were performed in the summer of 2012, and 9 street walks and 11 avenue walks were performed in the summer of 2013.

Fixed Instrument Campaigns

Ten Onset Corporation Hobo data loggers with temperature,relative humidity, and solar radiance sensors were deployed about Manhattan at the positions shown by the orange boxes in Fig. 1a. They were in white thermometer shelters mounted between 3.2 and 3.9 meters high on street light posts, and when possible placed directly above the street walk campaigns and in mid-day shadow. They were deployed from mid June through the beginning of October, 2013, collecting data every 3 minutes in order to capture temporal variability.

Instrument Comparisons

The instrument specifications from the manufacturer are given below. Note the much shorter response time of the temperature probe, which is nothing more than a thermocouple so has very low mass. The Hobo temperature and RH probes are integrated, providing similar response times.

	Resolution/Accuracy	**Response time**
Vernier *(mobile)*		(still/moving) air
Temperature	0.03 C / 0.3 C	60 sec / 10 sec
Relative Humidity	0.04% / 10%	60 min /40 sec
Hobo *(fixed)*		
Temperature	0.02 C/ 0.2 C	~ 5 minutes @ 1 m/s
Relative Humidity	0.1% / 2.5%	~ 5 minutes @ 1 m/s

Table 1: Instrument Specifications. Response times are the requirement for a 95% change between initial and final readings when conditions are changed.

Comparisons were made by placing all probes on a table within a 1 m^2 area, covered with a cardboard box to reduce variations due to radiation and convection. Measurements were made for 10 minutes, then the table was rotated and the procedure was repeated. Averages and deviations from the average were calculated for each set of instruments, and appear in Table 2.

The values show deviations within each instrument set; but the average values of the Vernier and Hobo instrument sets were within 0.05 degrees and 2% RH of each other. The differences between instruments sets were deemed negligible, but the differences within the Vernier instruments required correction, as the biases were large but stable compared to short term temporal variations.

	Vernier T (C)	Hobo T (C)	Vernier RH %	Hobo RH %
Avg deviation from mean	0.2	0.04	1.3	0.5
Max deviation from mean	0.35	0.05	3.6	0.74
Max10 min variability	0.03	0.03	0.33	0.6

Table 2: Controlled intercomparison of instrument sets.

Table 2 shows that the variations between Hobo instruments were much smaller than the Vernier variations, though similar in temporal variability. The Hobo instruments were therefore not bias corrected.

Data Processing

The goal of the dataset is a set of anomaly maps, averaged over the many days of the field campaigns. The data was processed in three steps:

Detrending: mobile measurements were taken over a roughly 40 minute time period, during which the average ambient temperature could change. This was addressed by finding the average temperature and dewpoint measurements at a number of MetNet stations on Manhattan (values at a single instrument were found to be unstable) at 2 pm and 3 pm, and linearly interpolating to find the average ambient temperature at any point in time. This was subtracted from measurements at each location to arrive at detrended measurements:

$$V_{dt}(x) = V(x,t) - V_{ref}(t) \qquad \textit{(data detrending)}$$

Where 'V' stands for the values of T, RH or DewPoint. Detrending was not applicable to the fixed station measurements for which all measurements were done in synchrony. For each set of measurements Manhattan-wide averages and standard deviations were calculated, and values at each point were differenced from the averages to form anomalies:

$$V_{diff}(x) = V_{dt}(x) - \langle V_{dt} \rangle \qquad \textit{(“differences”)}$$

The difference anomalies were then divided by the Manhattan-wide standard deviations to form normalized anomalies termed "deviations":

$$V_{dev}(x) = V_{diff}(x) / SD \qquad \textit{(“deviations”)}$$

The deviations represent the number of standard deviations each measurement is from the average, so that all measurements fall on a unit Gaussian distribution centered on zero. The differences and deviations for all days were averaged together to form average anomaly maps. The difference maps favor the larger amplitude days, while the deviation maps treat all days equally, preserving the pattern rather than the magnitude of the measurements.

The fixed instruments afforded an extra step of processing to isolate spatial and temporal variations in the measurements. Fair weather convective variability is on the order of 30 minutes or less. An hour average at each location will effectively eliminate temporal variability, and the differences between stations at the same time represents spatial variability alone. To represent how spatial variability changed with time, tables were made of the standard deviations calculated between hourly averages of all stations.

Temporal variability can be calculated by subtracting a 60 minute running average from the data and calculating standard deviations from these residuals (Figure 2). Tables were constructed of the standard deviation of the spatial variability over each hour of the field campaign for each of the 10 instruments.

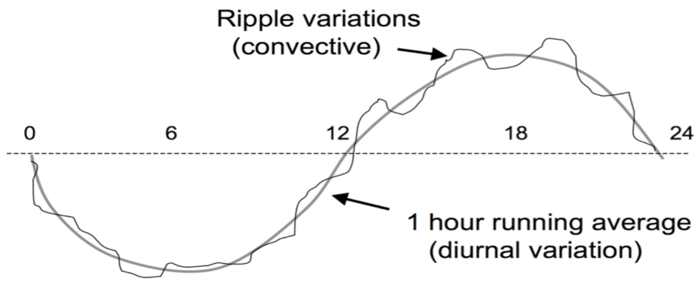

Figure 2: Calculation of temporal variation by subtracting a running average from the raw data.

Results

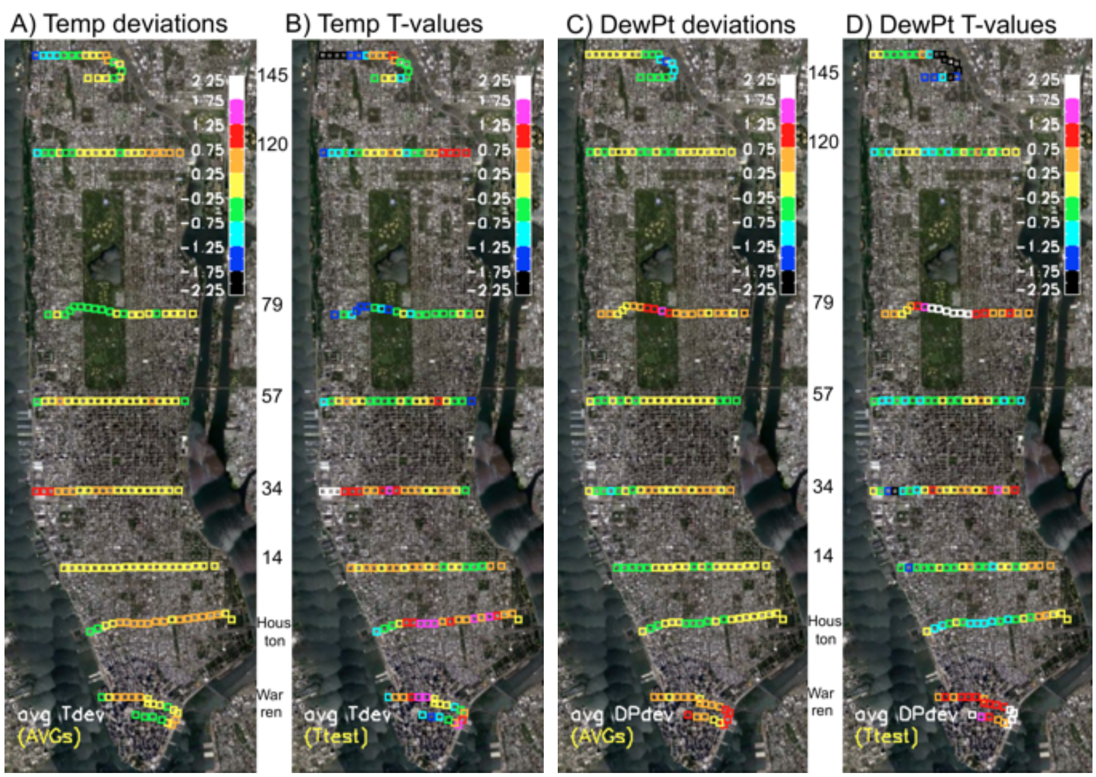

Figure 3: Street measurements of temperature and dewpoint anomalies. Each colored square in A and C represents the mean number of standard deviations from which the measurement varies from the Manhattan average on the day each measurement was taken. Note that yellow represents the average value with the red part of the spectrum representing above average and the blue side of the spectrum below average. The Student T values in B and D are calculated using the mean and standard deviation of the measurements at that point compared to an “average sample” with a mean of 0, a standard deviation equal to the average standard deviation, and a number of points equal to the number of days measurements were done. The T values are interpreted in table 3.

Symbol (positive) Colors (negative)					
T value	+/- 0.25	+/- 0.75	+/- 1.25	+/- 1.75	+/- 2.25
Confidence level	60%	77%	89%	97%	99%

Table 3: T values and Confidence levels for Figures 3 b,d and 4 b,d.

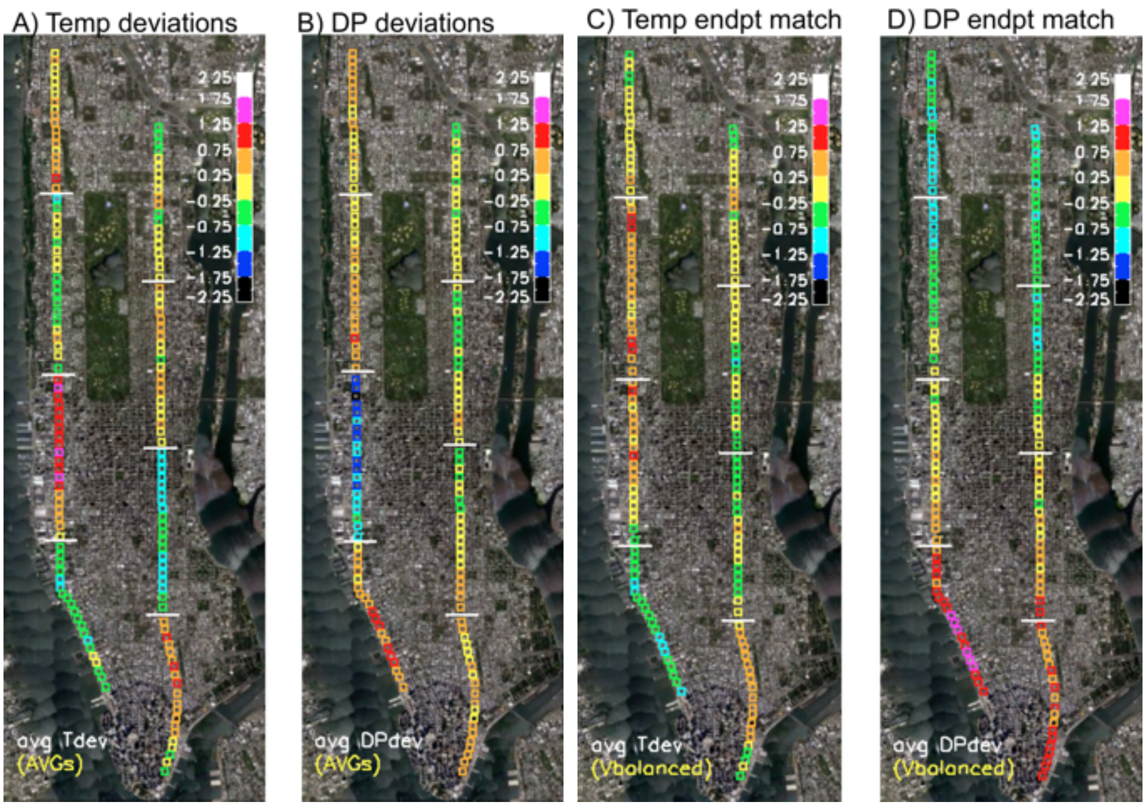

Figure 4: Temperature and dewpoint anomalies measured along avenues, with meanings for A and B as explained in figure 6. Boundaries between measurement routes are marked with white lines. The patchwork effect seen in A and B is likely due to solar heating of the relative humidity instrument, so endpoint matching is done in B, C. The procedure is described in the next section, but invalidates T-test calculations which are not shown.

Figure 3 shows averaged anomalies from the mobile campaigns, normalized by standard deviation ('deviation anomalies'). Temperature and dewpoint are shown with dewpoint used instead of relative humidity because it represents the absolute amount of water vapor in the air so is more stable against temperature fluctuations. The statistical quality of this data is evaluated by the Student T test, shown in panels B and D. Conversion of T values into confidence levels is based on the number of data points, and a conversion chart appears in Table 3.

Figure 4 shows temperature and dewpoint anomalies along the avenues. A distinct patchwork pattern is seen in panels A,B between the routes, attributed to insufficient shielding for the full sunlight the instruments were exposed to, and varying placement of the instrument packs to achieve a uniform 1.5 meter elevation on people of different heights. This was addressed by assuming constant biases (the same field workers were used on each route) and adjusting the

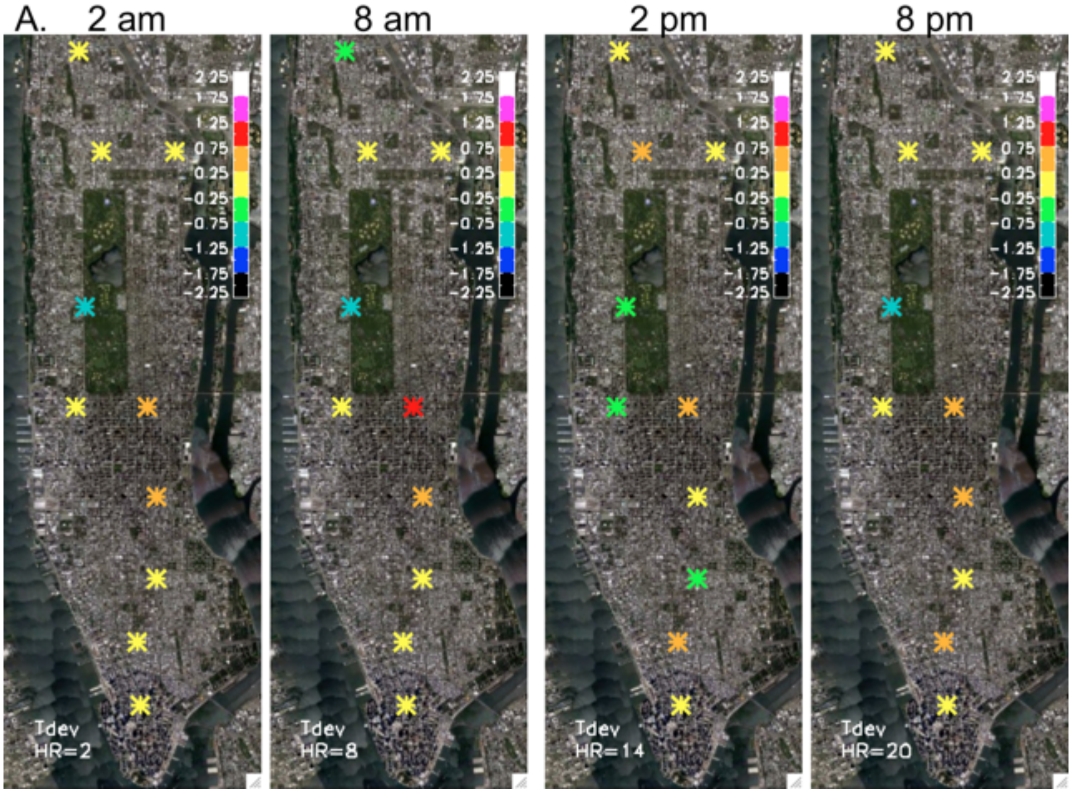

Figure 5 A: Temperature anomalies in standard deviations for selected hours.

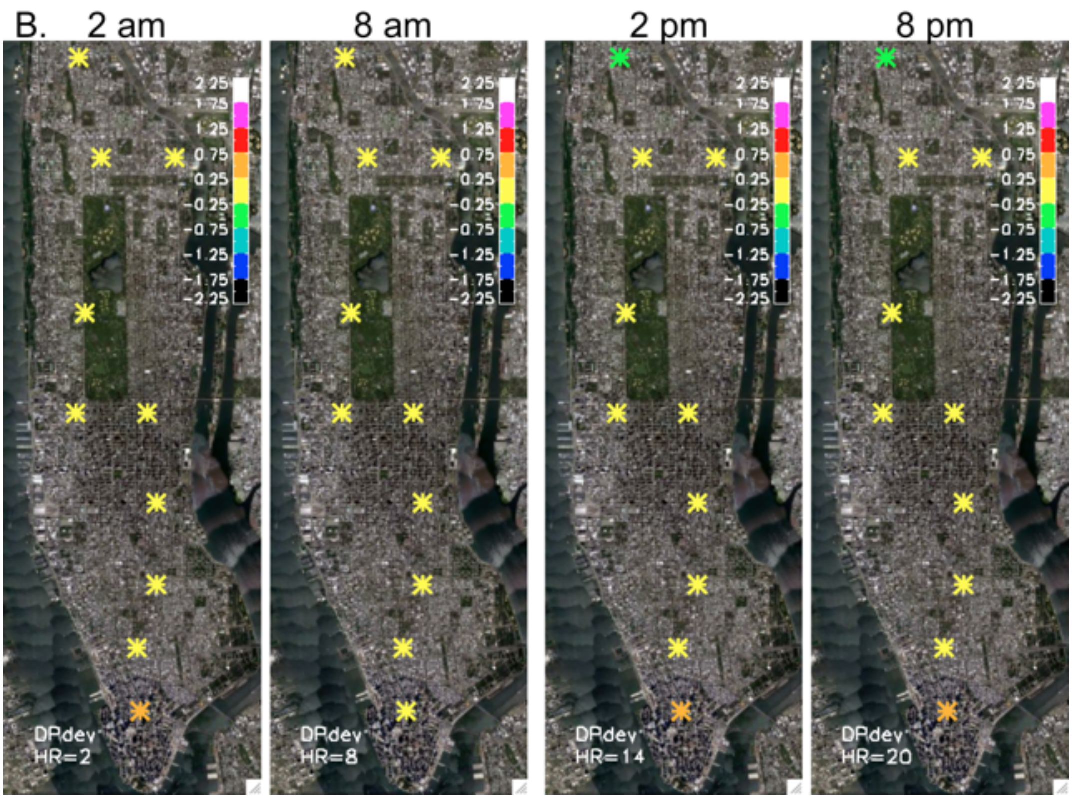

Figure 5 B: Dewpoint anomalies in standard deviations for selected hours.

biases so that the values were continuous at the route endpoints. The results of this adjustment is shown in panels C, D.

Anomaly maps made from the fixed stations appear in Figure 5, for every 6 hours throughout the diurnal cycle.

Physical Interpretations

When interpreting the maps of Figures 3 and 4 it is useful to recall that the average standard deviation seen in the mobile campaigns each day was about 1.1 C, so that the deviations can roughly be interpreted as temperature differences.

Some general trends are evident in the street data maps of Fig. 3. Temperature is lower in the Heights on the west ends of 145th and 120th streets, and higher in the low lying east sides of 120th and 14th streets. The cooling effects of vegetation can be seen while traversing parks on 120th street and 79th street, and while near water on 57th, Houston, and Warren streets. Lower buildings allowing greater street insolation may also be responsible for warmer areas on 34th, Houston and 120th streets. The dewpoint generally increases near water and vegetation, and decreases with elevation. These observations have been paired with albedo, NDVI, building parameters and proximity to water, but a full statistical analysis of the correlations and cross correlations between these variables is beyond the scope of this paper. Preliminary results show that for the street data the strongest temperature correlation is to altitude, followed by vegetation (NDVI), building parameters and proximity to water.

The patchwork correction scheme applied to Fig 4 appears in panels C, D. In general the temperatures are lowest and dewpoints are highest near water, and with the exception of warm temperatures seen on the Upper West Side the trend of temperature and dewpoints dropping with elevation is also seen.

These visual impressions are borne out by statistical regression against surface variables. Though such an analysis is beyond the scope of the current paper, preliminary results show that for the shaded street data the strongest temperature correlation is to altitude, followed by vegetation (NDVI), building parameters and proximity to water. For the sunlight avenues the strongest correlation is to albedo, followed by vegetation and building height. The effects of building height in avenues are opposite to the shaded street data: in the streets higher buildings have a cooling effect, while in the sunny avenues higher buildings have a warmer effect, likely due to increased reflection, for the albedo switches correlations to relate higher temperatures to higher absorption in the streets and higher reflection in the avenues.

The fixed instrument anomalies of Figure 5 are similar to Figure 3 at the 2 pm hour, though with differences in magnitude as expected for a smaller sample set (the average spatial standard deviation was about 0.3 C). The dewpoints are far more uniform than the temperatures, with noticeably higher dewpoints at the tip of Manhattan surrounded with water, and lower dewpoints in Heights to the North.

Comparisons between the two data sets are best understood if the relationship between the variability seen in both instrument sets is clarified. The mobile campaigns experienced combined spatial and temporal variability which should be reflected in the separated components of variability calculated from the fixed campaign. To explore this the two modes of the fixed variability were plotted against the total variability of the mobile campaigns, compared day by day. This is shown in Figure 6. We see in Fig. 6 a,b that the relationship between the total mobile variability and two components of the fixed campaign are weak, but when combined the correlation improves and the relationship becomes a simple proportionality (zero intercept). This understanding can be used to compare the fixed and mobile data sets.

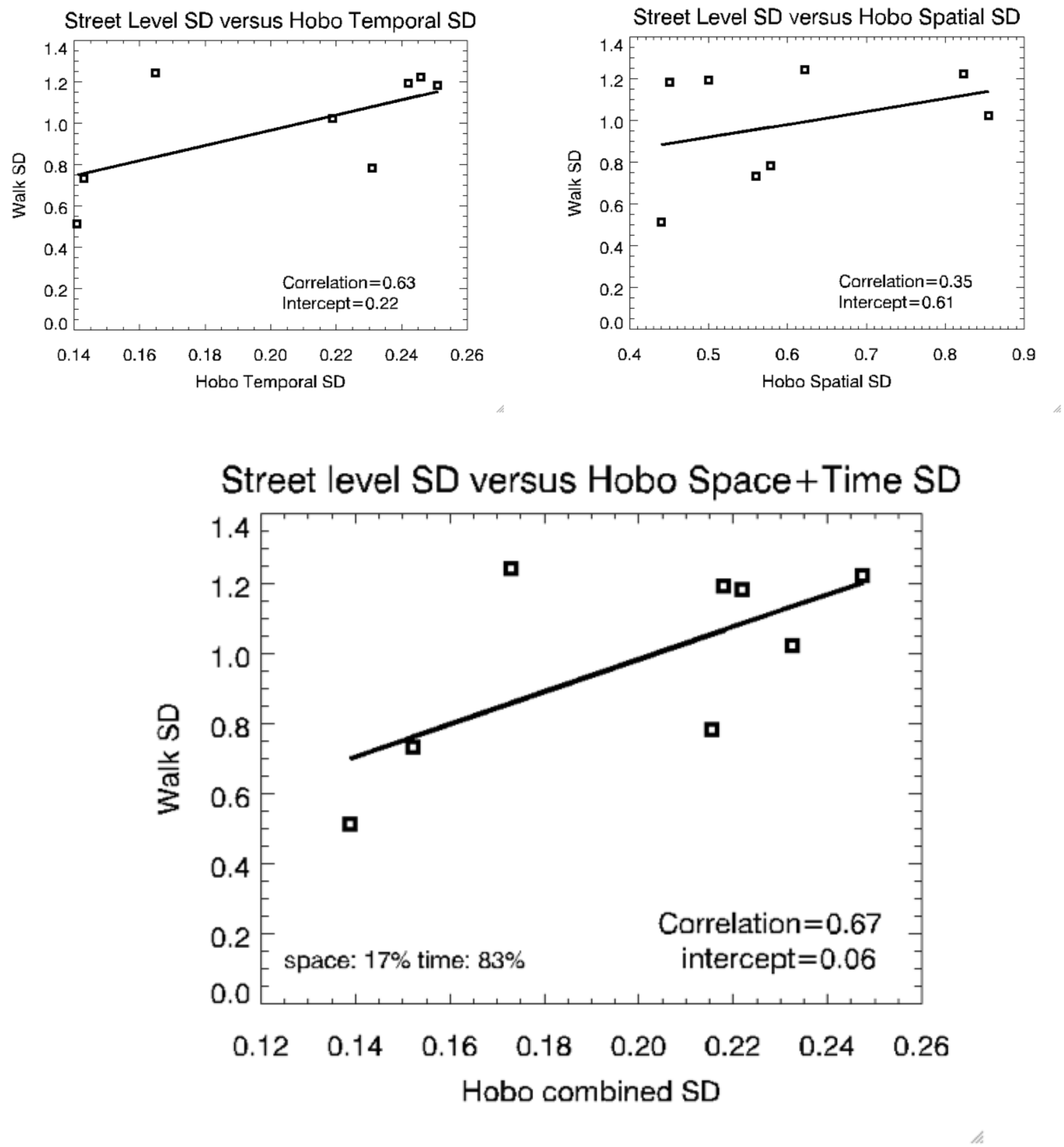

Figure 6: Variability in mobile temperature measurements versus spatial and temporal variability in fixed Hobo instrumentation for 8 different days. Standard Deviations of the mobile instrument measurements are plotted versus: (Top Left) Hobo spatial variations. (Top Right) Hobo temporal variations. (Bottom) Vector combination of Hobo spatial and temporal variations

Perhaps the largest disagreement when comparing the mobile and fixed data sets of Figures 3 and 5 is the switch in the East-West temperature gradient seen on 120th street (second from the top). This could arise from comparing single point measurements to the mobile averages over a distance of roughly 150 meters. Another apparent difference is the warm and cool points seen on 57th street (directly below Central Park) in the fixed data, while the mobile campaigns show a more uniform range. Since the spatial variance of the fixed stations were typically smaller than the total variance seen in the mobile campaigns (0.5 C versus 1.1 C; much of it temporal in the mobile campaigns), the result is that what may look like large variations in the fixed campaign fall within in the average range shown for the mobile campaigns.

Data Availability

All data and imagery derived from it is available at the project website:

http://glasslab.engr.ccny.cuny.edu/u/brianvh/UHI

The high temporal variability seen in the mobile campaigns means the data from any single day is not representative of the averaged pattern. For this reason only the averaged mobile data is made available. All data from the fixed campaigns are available as the interpretation is more straightforward. In addition the measures of variability and hourly averages for the fixed campaigns are included.

The average spatial patterns seen in the temperature and dewpoint maps are attributed to spatial variations in surface cover. For this reaon gridded maps of albedo, vegetation (NDVI), building parameters, elevation and water fraction are provided, and are matched to each point in the mobile campaign data. The data sources will be updated as improved version are processed, so at this point description of these sets are left to the website to be updated as needed.

Conclusions

A new dataset characterizing the Manhattan urban heat island has been produced by a combination of street level mobile campaigns measuring Temperature (T) and Relative Humidity (RH) at high spatial resolution, and fixed instrumentation measuring T, RH and downwelling radiance at high time resolution. The mobile campaigns occurred during the summers of 2012 and 2013 while the fixed measurements occurred across 3 months in the summer of 2013.

The datasets are unique not only by virtue of their high spatial and temporal resolution, but by being normalized by standard deviation before being averaged, capturing the pattern of the variability rather than the magnitude.

Data and imagery from these camapaigns are available at the project website:

http://glasslab.engr.ccny.cuny.edu/u/brianvh/UHI

Acknowledgements: This work was supported in part by NOAA grant NA11SEC481004 to the Cooperative Remote Sensing Science and Technology (CREST) Institute at the City College of New York, and by NOAA Regional Integrated Science Assessment (RISA) award #NA10OAR4310212 to the Consortium for Climate Risk in the Urban Northeast (CCRUN). The authors gratefully acknowledge data and imagery made available for fair use by NYC MetNet, the National Building Statistics Database, the US Geological Survey, and Google Earth.

References

Bottyán, Z. and J. Unger, "A multiple linear statistical model for estimating
the mean maximum urban heat island," Theo. Appli.Clim., vol.

Comrie, A. C., 2000: *Mapping a wind-modified urban heat island in Tucson, Arizona (with comments on integrating research and undergraduate learning).* Bull. Amer. Meteor. Soc., 81, 2417–2431.

Eliasson, Ingegard, 1996a: *Intra-urban nocturnal temperature differences: a multivariate approach.* Climate Research V 7, pp 21-30.

Eliasson, Ingegard. 1996b: *Urban nocturnal temperatures, street geometry and land use*, Atmos. Environ., V 30, 379–392.

Gaffin, S.R., Rosenzweig, C., Khanbilvardi, R., Parshall, L., Mahani, S., Glickman, H., Goldberg, R., Blake, R., Slosberg, R.B. and Hillel, D., 2008: *Variations in New York City's Urban Heat Island Strength Over Time and Space*, Journal of Theoretical and Applied Climatology, V 94: 1–11

Grimmond, Sue, 2007: *Urbanization and global environmental change: local effects of urban warming.* In *Cities and global environmental change,* Royal Geographic Society, London.

Grimmond, C.S.B, and T. Oke, 1999: *Heat storage in urban areas: local-scale observations and evalutation of a simple model.* J. Appl. Meteor. V 38, 922-940.

Kinney, P., P. Sheffield, r. Ostfeld, J. Carr, R. Leichenko, P. Vancura, 2008a: *Public Health.* New York State Energy Research and Development Agency (NYSERDA) Report 11-18: Response to Climage Change in New York State (ClimAID). Chapter 11. http://www.nyserda.ny.gov/climaid

Kinney, P., M. O'Neill, M. Bell, J. Schwartz, 2008: *Approaches for estimating effects of climate changes on heat related deaths: challengebs and opportunities.* Environmental Science and Policy. Volume 11, 87-96.

Montavez JP, Rodrıguez A, Jimenez JI, 2000: *A study of the urban heat island of Granada*. Int J Climatol 20: 899–911

Oke, T.R., 1982*: The energetic basis of the urban heat island*, Quart. J. Roy. Meteorol. Soc., vol. 108, pp. 1–24

Pena, Marco, 2009: *Examination of the Land Surface Temperature Response for Santiago, Chile.* Photogrammetric Engineering & Remote Sensing, Vol. 75, No. 10, October 2009, pp. 1191-1200.

Rosenzweig C, Solecki W, Parshall L, Gaffin S, Lynn B, Goldberg R, Cox JS Hodges (2006) Mitigating New York City's heat Island with urban forestry, living roofs and light surfaces, in Proceedings of the 86th Annual Meeting of the American Meteorological Society, Jan 29–Feb 2, 2006, Atlanta, GA

Stewart, Iain, Tim Oke: 2009: *Newly developed "Thermal Climate Zones" for defining and measuring urban heat island magnitude in the canopy layer.* Am. Met. Soc. Annual Meeting, Phoenix, AZ, 2009. http://ams.confex.com/ams/pdfpapers/150476.pdf .

Weng, Qihao, D. Lu, and Jacquelyn Schubring, 2003: *Estimation of land surface temperature-vegetation abundance relationship for urban heat island studies.* Remote Sensing of the Environment, V 89, pp 467-83.

Weng, Qihao, H. Liu, B. Liang, D. Lu, 2008: *The spatial variations of urban land surface temperatures: pertinent factors, zoning effect, and seasonal variability.* IEEE J. sel topics in appl. Earth obs rem sens. Vol 1 n 2, 154-166

Weng, Qihao, 2009: *Thermal infrared sensing for urban climate and environmental studies: methods, applications and trends.* IPRS J. Photgram. Rem. Sens. V 64, 335-344.

Yamashita, S. 1996: *Detailed structure of heat island phenomena from moving observations from electric tram-cars in metropolitan area*, Atmos. Environ., 30, 429–435.